A study of cell-to-cell variation of capacity in parallel-connected lithium-ion battery cells

Ziyou Song [a, b], Xiao-Guang Yang [c, *], Niankai Yang [a], Fanny Pinto Delgado [b], Heath Hofmann [b], Jing Sun [a]

[a] Department of Naval Architecture and Marine Engineering, University of Michigan, Ann Arbor, MI, 48109, USA
[b] Department of Electrical Engineering and Computer Science, University of Michigan, Ann Arbor, MI, 48109, USA
[c] Department of Mechanical and Nuclear Engineering and Electrochemical Engine Center (ECEC), The Pennsylvania State University, University Park, PA, 16802, USA

ARTICLE INFO

ABSTRACT

Capacity variation among battery cells can occur due to inconsistent manufacturing processes and operating conditions, such as uneven temperature distribution. For a battery string made of parallel-connected cells with only one voltage and one current sensor, the lack of independent current sensors makes it difficult to detect or control the degradation variation. In order to investigate the progression mechanism of cell-to-cell capacity variation, this paper adopts an electric aging model and analytically determines the relationship between variation progression and cell degradation characteristics. Assuming all cells have similar temperatures, the capacity variation will decrease over time for cells with a convex or linear degradation curve (i.e., the most common case), providing a self-balancing mechanism for parallel-connected cells. Compared to battery strings with uniform cell capacities, battery strings with an initial cell-to-cell variation will degrade slightly faster. State-of-charge imbalance and uneven heat generation are analyzed using a thermal model. Assuming the same coefficient of heat transfer (i.e., same cooling condition), simulation results further verify the self-balancing mechanism for a parallel battery string consisting of 5 LiFePO4 battery cells.

© 2020 Elsevier B.V. All rights reserved.

1. Introduction

Lithium-ion batteries have been widely used in electrified vehicles, such as plug-in hybrid electric vehicles (PHEVs) and electric vehicles (EVs) [1], and renewable energy systems such as wind farms [2]. To maximize battery pack capacity under space and cost constraints, battery cells are often connected in parallel to form battery strings, which become the building blocks for battery modules or packs [3]. For example, the battery packs of Nissan Leaf, Chevrolet Volt, BMW E-Mini, and Tesla Model S have 2, 3, 53, and 74 cells connected in parallel, respectively [4,5]. Unlike series-connected battery cells, where both voltage and current measurements of a single cell are typically available [6], it is difficult to determine the condition of parallel-connected cells since generally only one voltage sensor and

one current sensor are used per string [7]. The lack of current sensors for individual cells results in low observability and no controllability of the healthy condition of individual cells. Cell-to-cell capacity variation is therefore difficult to detect and control.

Capacity (i.e., the general indicator of State of Health (SoH)) variation among different cells caused by manufacturing inconsistency [8] or uneven temperature distribution [9] will result in resistance variations which are highly associated with battery degradation [10]. Both capacity and resistance variations lead to current imbalance among cells connected in parallel, which will in turn cause different aging rates among cells [11]. Given the inevitable initial cell-to-cell variation, understanding how this variation evolves over time, and how it may impact battery performance and degradation, is very important, particularly for applications involving large battery packs; e.g., so-called "second-life" battery packs with cells of different capacities for renewable energy applications [12,13].

The aging of battery strings consisting of non-uniform cells has been addressed in the literature. Paul et al. [14] studied series-

---

connected battery cells considering variations in initial capacity, initial internal resistance, aging rate, and thermal coupling, and simulation results show that discrepancies in cell aging are the consequence of uneven current distribution. Chiu et al. [15] also focused on series-connected battery cells and verified that capacity degradation increases with an increase in temperature variation. For parallel-connected battery cells, Offer et al. [16] tested a lithium-ion battery pack in a vehicle environment and reported that different inter-cell contact resistances can cause currents to flow unevenly within the pack, leading to cells being unequally loaded. Bruen and Marco [3] experimentally evaluated the imbalance of parallel-connected cells and reported the results of a 30% difference in impedance, 60% difference in peak cell current, and over 6% difference in charge throughput during cycling. Fernández et al. [4] conducted experiments on four lithium-ion battery cells connected in parallel at 25 °C and showed that an initial SoH difference of 40% converges to 10% after 500 cycles. Shi et al. [5] analyzed the imbalance currents of parallel LiFePO$_4$ battery systems and pointed out that fast aging can be avoided by suppressing variations of temperatures and branch currents. Yang et al. [17] showed that unbalanced discharging and aging can be caused by temperature differences between parallel-connected battery cells. Gong et al. [18] concluded that, with cells with different levels of degradation in parallel, there can be a large difference in discharge which can result in accelerated degradation and a more serious inconsistency problem. Liu et al. [19] adopted a thermal single-particle model to study a parallel battery string, and found that uneven overpotentials caused by the interconnects and temperature gradients significantly influence the battery pack performance.

The progression of cell-to-cell variation among parallel-connected battery cells over time as individual cells are aging has been discussed in the above studies with some conflicting conclusions. For example, capacity variation is found to diminish in Ref. [4], while it is found to increase in Ref. [18]. Note that the conclusion in Ref. [18] is deduced from indirect testing results (e.g., temperature distribution) rather than direct experimental result or theoretical analysis. In addition, no theoretical analysis has been provided on this topic to the best of our knowledge. It is intuitive to use identical or similar cells in one battery string; however, the benefit of doing so has not been characterized or quantified.

To this end, this paper carries out an analytical investigation using a thermal electric aging model to understand the impact of the cell-to-cell variations of current, degradation rate, State of Charge (SoC), and heat generation over the short term, and capacity over the long term. Given an initial cell-to-cell variation, the current distribution caused by the resistance imbalance is analyzed based on an electric model of parallel-connected cells. Furthermore, the current imbalance is used as an input to a battery degradation model to investigate the degradation rates of different cells. The results show that the progression of the cell-to-cell variation is directly determined by the cell degradation characteristics. Assuming all cells have similar temperatures, the capacities will converge over time for cells with convex or linear degradation curves. This means that parallel-connected cells in these conditions have a self-balancing mechanism. We point out that the temperature distribution within the battery string also influences cell-to-cell variation, but this is an independent and complex topic given the very different cooling structures available in vehicles [20]. Assuming the linear degradation characteristics of battery cells, it can be shown that capacity variation increases the total degradation of the battery string when compared to a battery string with the same total capacity and no variation. In addition, SoC imbalance and uneven heat generation among different cells are also analyzed. Simulations are conducted under the assumption of homogeneous cooling, and the results further verify the self-

balancing mechanism and the slight benefit of adopting identical/similar cells in one battery string.

The rest of the paper is organized as follows. In Section 2, a battery string model, including an electric model, degradation model, and thermal model, is introduced. In Section 3, analysis is presented to show the dynamic behavior and impact of cell-to-cell variations. Simulation results are provided in Section 4. Discussion is given in Section 5. Conclusions are then drawn in Section 6.

2. Battery string modeling

Consider a battery string which consists of N cells connected in parallel with different initial capacities, as shown in Fig. 1. One voltage sensor, which measures the terminal voltage for all cells, and one current sensor, which measures the total current, are used. The individual current of each cell is unknown. We first investigate the current distribution based on an electric model of the battery string.

2.1. Electric model

The first-order equivalent circuit model (ECM), as shown in Fig. 1, is used to represent the dynamics of an individual cell given its simplicity and sufficient accuracy [21]. The ECM dynamics are described as:

$$\begin{cases} \dot{v}_{Cj} = -\dfrac{1}{\tau_j}v_{Cj} + \dfrac{R_{ti}}{\tau_i}i_{bj}, \\ v_b = v_{OCj} - R_{si}i_{bj} - v_{Cj}, \end{cases} \quad j = 1,\, 2\cdots N \quad (1)$$

where v_{OC} is the open circuit voltage (OCV), v_b is the terminal voltage, i_b the cell current (positive for discharging and negative for charging), R_s is the ohmic resistance, R_t, τ, v_C are the resistance, time constant, and voltage of the RC pair, respectively, and j denotes the cell number. The terminal voltage v_b of each individual cell is the same. The OCV-SoC curve is generally nonlinear within the entire SoC region [22] but with a constant slope within the normal operating range for most battery chemistries [23–25]. Therefore, we use a linearized OCV-SoC relationship in our analysis which has the expression of

$$v_{OCi}(t) = a \cdot SoC_i(t) + b \quad (2)$$

where t is time, and a and b are the coefficients of the linearized OCV-SoC function, which is assumed to be constant regardless of temperature and degradation level. The influence of cell degradation on the OCV-SoC function will be further discussed in the sequel. The SoC dynamic is given by Refs. [26]:
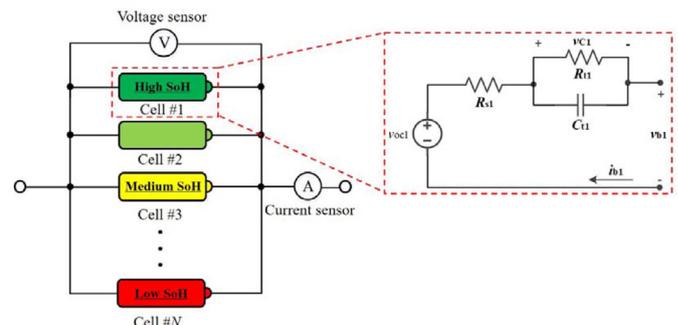
Fig. 1. The parallel-connected battery cells with initial capacity variation.

$$SoC_j(t) = SoC_j(0) - \int_0^t \frac{\eta}{Q_{bj}} i_{bj}(t)dt \tag{3}$$

where Q_b is the cell capacity and η is the charge/discharge efficiency. Based on Eqs. (1)–(3), the state space representation of the battery cell dynamics can be derived as:

$$\begin{bmatrix} \dot{v}_{OCj} \\ \dot{v}_{Cj} \end{bmatrix} = \begin{bmatrix} 0 & 0 \\ 0 & -\frac{1}{\tau_j} \end{bmatrix} \cdot \begin{bmatrix} v_{OCj} \\ v_{Cj} \end{bmatrix} + \begin{bmatrix} \alpha_j \\ \frac{R_{tj}}{\tau_j} \end{bmatrix} \cdot i_{bj} \tag{4}$$

$$v_b = \begin{bmatrix} 1 & -1 \end{bmatrix} \cdot \begin{bmatrix} v_{OCj} \\ v_{Cj} \end{bmatrix} - R_{sj} \cdot i_{bj} \tag{5}$$

where $\alpha_j = -\frac{a\eta}{Q_{bj}}$. The analysis in the next section will focus on a 2-cell case, which is the simplest case, with the following dynamic model:

$$\dot{x}_s = A \cdot x_s + B \cdot \begin{bmatrix} i_{b1} \\ i_{b2} \end{bmatrix} \tag{6}$$

$$v_b = C \cdot x_s + D \cdot \begin{bmatrix} i_{b1} \\ i_{b2} \end{bmatrix} \tag{7}$$

where

$$x_s = \begin{bmatrix} v_{OC1} & v_{C1} & v_{OC2} & v_{C2} \end{bmatrix}^T, \quad A = \begin{bmatrix} 0 & 0 & 0 & 0 \\ 0 & -\frac{1}{\tau_1} & 0 & 0 \\ 0 & 0 & 0 & 0 \\ 0 & 0 & 0 & -\frac{1}{\tau_2} \end{bmatrix}, \quad B = \begin{bmatrix} \alpha_1 & 0 \\ \frac{R_{t1}}{\tau_1} & 0 \\ 0 & \alpha_2 \\ 0 & \frac{R_{t2}}{\tau_2} \end{bmatrix},$$

$$C = \begin{bmatrix} 1 & -1 & 0 & 0 \end{bmatrix}, \quad D = \begin{bmatrix} -R_{s1} & 0 \end{bmatrix}.$$

According to Kirchhoff's laws, the relationship between the battery string current i_b (i.e., total current) and the individual cell currents are given as

$$R \cdot \begin{bmatrix} i_{b1} \\ i_{b2} \end{bmatrix} = E \cdot x_s + F \cdot I_b \tag{8}$$

where

$$R = \begin{bmatrix} 1 & 1 \\ -R_{s1} & R_{s2} \end{bmatrix}, \quad E = \begin{bmatrix} 0 & 0 & 0 & 0 \\ -1 & 1 & 1 & -1 \end{bmatrix}, \quad F = \begin{bmatrix} 1 \\ 0 \end{bmatrix}.$$

Based on Eq. (8), the current distribution can be determined as follows

$$\begin{bmatrix} i_{b1} \\ i_{b2} \end{bmatrix} = R^{-1} E \cdot x_s + R^{-1} F \cdot i_b \tag{9}$$

Finally, the entire electric model of the parallel battery string can be presented.

$$\dot{x}_s = \left(A + BR^{-1}E \right) \cdot x_s + BR^{-1}F \cdot i_b \tag{10}$$

$$v_b = \left(C + DR^{-1}E \right) \cdot x_s + DR^{-1}F \cdot i_b \tag{11}$$

2.2. Degradation model

The capacity and other features of a lithium-ion battery change over time, and this degradation process is characterized by an approximately linear region and a highly nonlinear region [27]. The linear region represents gradual decay due to the growth of solid electrolyte interphase (SEI), while the highly nonlinear region corresponds to fast decay at the end of battery lifetime with rapid capacity drop and resistance rise [28], induced by a sharp rise in the lithium plating rate [27]. In EV applications, the battery should be replaced when the capacity drops to 80% of the initial capacity [29]; i.e., before the start of its nonlinear degradation. Therefore, in this study, we focus only on the linear region. Wang et al. proposed a battery degradation model considering the effects of time, temperature, depth of charge, and discharge rate [31]. This model is based on Arrhenius degradation:

$$Q_{loss} = \frac{Q_{non} - Q_b}{Q_{non}} = Ae^{-\left(\frac{E_a + B \cdot C\_Rate}{RT_b} \right)} (A_h)^z, \tag{12}$$

where Q_{loss} is the normalized capacity loss, Q_{non} is the nominal capacity, A is the pre-exponential factor, E_a is the activation energy (J), R is the gas constant (J/(mol · K)), T_b is the absolute temperature (K), A_h is the amp-hour-throughput, C_Rate is the charge/discharge rate, z is the constant time factor indicating how the degradation rate changes over time, and B is the compensation factor. Eq. (12) can be expressed as a dynamic equation as follows:

$$Q_{loss}(t+1) - Q_{loss}(t) = \Delta A_h z A^{\frac{1}{z}} e^{-\left(\frac{E_a + B \cdot C\_Rate}{z RT_b} \right)} Q_{loss}(t)^{\frac{z-1}{z}}, \tag{13}$$

where

$$\Delta A_h = \frac{1}{3600} \int_t^{t+1} |i_b| dt.$$

Detailed information on the model discretization and experimental validation are provided in Ref. [29]. The time factor z directly determines the degradation characteristics. If z is less than 1, the battery degradation will slow down with time (i.e., convex degradation curve). If z is equal to 1, the battery will age at a
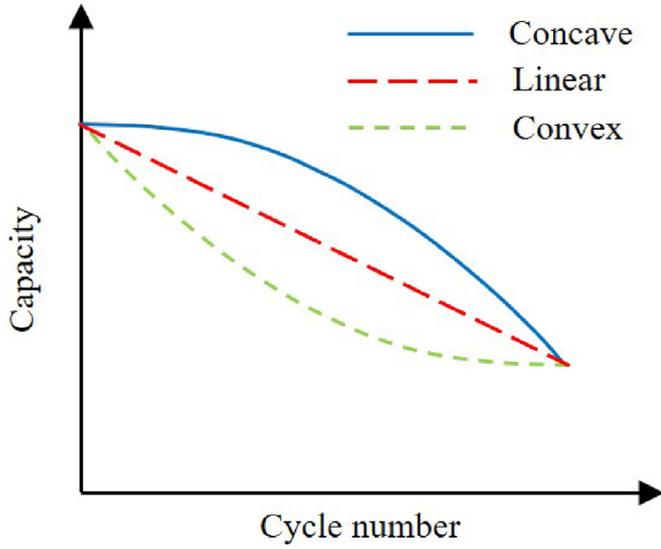
Fig. 2. Different degradation characteristics.

constant rate (i.e., linear degradation curve). If z is larger than 1, the battery degradation will accelerate with time (i.e., concave degradation curve). The comparison of different degradation characteristics is shown in Fig. 2.

It is widely acknowledged that the capacity loss of Li-ion batteries typically is convex regardless of the cathode chemistry [29,30]. Lithium iron phosphate (LFP) LiFePO4 batteries with different capacities have been extensively investigated in the literature [29−32]. In addition, lithium nickel-cobalt-manganese (NCM) oxide and lithium manganese oxide (LMO) have also been investigated and show convex degradation characteristics [27]. Cell aging is mainly dominated by the anode, and is ascribed to the growth of the SEI on the anode graphite surface. The rate of SEI growth depends on the rate of ethylene carbonate diffusion across the SEI film, which is fast at the beginning when the film is thin, and gradually levels out as the film thickens, leading to a convex shape of the capacity loss (i.e., $z < 1$). Note that when the battery reaches end-of-life, its degradation rate will significantly increase and the degradation curve will be concave [27]. However, this paper only focuses on the cell-to-cell variation in the normal lifetime of battery, so the concave degradation curve will not be considered.

2.3. Thermal model

As shown in Eq. (13), temperature also influences the battery degradation rate. Therefore, a thermal model of a battery cell is used in this study. A simplified heat generation model, considering joule heat and reaction heat, is given below [33]:

$$\dot{q}_{bj} = i_{bj}\left(v_{OCj} - v_{bj}\right) + i_{bj}T_{bj}\frac{\partial v_{OCj}}{\partial T_{bj}}, \qquad (14)$$

where $\dot{q}_b$ is the heat generation rate. The reaction heat is determined by the cell current and the effective entropic potential (i.e., $\partial v_{OCj}/\partial T_{bj}$), which is strongly influenced by SoC. Considering heat dissipation, the complete thermal model of battery cell can be described as

$$C_{bj}T_{bj}(k+1) = T_{bj}(k) + \left(\dot{q}_{bj} - h_{bj}\left(T_{bj} - T_{cj}\right)\right)T_s, \qquad (15)$$

where T_s is the sampling time, C_{bj} is the thermal capacity of the battery cell, h_{bj} is the heat transfer coefficient, and T_{cj} is the coolant temperature for the jth cell. Note that the cell temperature depends on both heat generation and heat removal. The heat removal of different cells varies with h_b and T_c, which are dictated by the cooling structure. Therefore, the parameters h_{bj} and T_{cj} are difficult to characterize, and are very dependent on pack design [34].

The thermal model shown in Eqs. (14) and (15) will be used in this study; however, we point out that the optimal temperature of the battery cell depends upon the chemistry and the load cycle characteristics [35]. Given that the optimal temperature can vary over a wide range (i.e., ~10 °C to > 30 °C) [35,36], it is difficult to address how the increasing temperature influences battery degradation for different chemistries. As a result, the temperature gradient in the battery string should be considered as an independent topic. In the analysis in Section 3 the temperature variation is not considered, given cooling structures in practical applications vary substantially, while the heat generation rates of different cells are analyzed.

3. Theoretical analysis

In this section, the current imbalance and cell-to-cell variations in SoC, heat generation, and degradation rate are analyzed based on the thermal electric aging model introduced in Section 2. A two-cell case is chosen at first to simplify the analysis. We consider two cells with different initial capacities, and assume that cell #1 has a lower capacity than cell #2 due to degradation, namely:

$$\begin{cases} Q_{b1} + Q_{b2} = Q_{bs}, \\ Q_{b2} = c \cdot Q_{b1}, \end{cases} \qquad (16)$$

where Q_{bs} is the total capacity of two cells and c is the capacity ratio between two cells (i.e., $c > 1$). This analysis applies to two cells with different capacities, regardless of total capacity and capacity ratio. In addition, while the cell resistance is influenced by many factors such as temperature and SoC, it significantly increases with degradation [37]. For example, the ohmic resistance of a lithium-ion battery cell can increase by more than 200% when the cell capacity degrades to 85% of the initial value at 25 °C [38]. Therefore, both the ohmic resistance R_s and the diffusion resistance R_t are assumed to increase more quickly than degradation in this paper, i.e.:

$$R_{sj} = \varepsilon \left(\frac{Q_0}{Q_{bj}}\right)^{\lambda} R_{s0},$$

$$R_{tj} = \varepsilon \left(\frac{Q_0}{Q_{bj}}\right)^{\lambda} R_{t0}, \qquad (17)$$

where both ε and λ are constant coefficients ($\varepsilon > 1$, $\lambda \geq 1$), Q_0 is the nominal capacity, and R_{s0} and R_{t0} are the nominal ohmic resistance and diffusion resistance corresponding to the fresh cell, respectively. As shown in Eq. (17), the battery resistance is assumed to exponentially increase with degradation. This is a general form describing the resistance increase and can be fitted to actual data. Note that the influence of temperature is not quantitatively considered in the analysis, for reasons mentioned in Section 2.3. Furthermore, the OCV-SoC relationship is assumed to be constant

with respect to degradation, as verified in many existing studies [39–43].

3.1. Current imbalance

When two battery cells have been connected in parallel after a long standing period, the following initial conditions are achieved:

$$v_{C1}(0) = v_{C2}(0) = 0,$$
$$v_{OC1}(0) = v_{OC2}(0) = v_b(0),$$
$$SoC_1(0) = SoC_2(0).$$
(18)

Note that when OCV does not degrade with the decreasing cell capacity, the cell voltage after equilibration will be in the acceptable range as long as all individual voltages are normal. However, when there is significant degradation in OCV, the voltage of lower-capacity cell in high SoC range may be above its maximum voltage after equilibration. Similarly, the voltage of higher-capacity cell in low SoC range may be below its minimum voltage after equilibration. This issue will be further elaborated in Section 5. To better understand the uneven distributions of cell current, heat generation, and SoC variation, analysis is conducted in the frequency domain. Consider a current i_b flows into the battery string. The following relationships can be obtained based on the circuit shown in Fig. 1.

$$I_{b1}(s) + I_{b2}(s) = I_b(s),$$
$$V_b(s) = V_{OC1}(s) - Z_1(s)I_{b1}(s)$$
$$= V_{OC2}(s) - Z_2(s)I_{b2}(s),$$
(19)

where
$$Z_1(s) = \left(R_{s1} + \frac{R_{t1}}{1 + s\tau_1}\right),$$
$$Z_2(s) = \left(R_{s2} + \frac{R_{t2}}{1 + s\tau_2}\right),$$
and s is Laplace variable and $Z_1(s)$

and $Z_2(s)$ are the cell impedances. Note that in this section OCV-SoC relationship is assumed to be constant and the time constants of different cells (i.e., τ_1 and τ_2) are assumed to be same. Therefore, based on Eqs. (2) and (3) we have

$$V_{OC1}(s) = a\left(\frac{SoC_1(0)}{s} - \frac{\eta}{sQ_{b1}}I_{b1}(s)\right) + b,$$
$$V_{OC2}(s) = a\left(\frac{SoC_2(0)}{s} - \frac{\eta}{sQ_{b2}}I_{b2}(s)\right) + b.$$
(20)

According to Eqs. (16)–(20), the current distribution in the frequency domain can be derived as

$$I_{b1}(s) = \frac{Z_2(s) + \frac{a\eta}{sQ_{b2}}}{(1 + c^\lambda)Z_2(s) + (1 + c)\frac{a\eta}{sQ_{b2}}},$$

$$I_{b2}(s) = \frac{c^\lambda Z_2(s) + c\frac{a\eta}{sQ_{b2}}}{(1 + c^\lambda)Z_2(s) + (1 + c)\frac{a\eta}{sQ_{b2}}}.$$
(21)

This shows that the current of the higher-capacity cell i_{b2} is larger and the resistance ratio (i.e., $R_{s2}/R_{s1} = c^{-\lambda}$) significantly influences the transient response of current distribution (i.e., $s \to \infty$), while the capacity ratio (i.e., $Q_{b2}/Q_{b1} = c$) dominates the steady-state response of current distribution (i.e., $s \to 0$). If the current profile contains high-frequency content the current distribution mainly depends on the cell resistance since the ohmic resistance dominates the high-frequency voltage response of the battery cell [22]. In addition, given that $\lambda \geq 1$, the following relationship on the amplitudes of individual cell currents can be given by

$$|i_{b2}(j\omega)| \geq c|i_{b1}(j\omega)|.$$
(22)

The joule heat, which generally dominates the heat generation [44], is also analyzed for different cells. Based on Eqs. (17) and (22), the uneven joule heat generation within the battery string can be shown as

$$\dot{q}_{b2} = \text{Re}[z_2(j\omega)]|i_{b2}(j\omega)|^2 \geq \frac{c^2}{c^\lambda}\text{Re}[z_1(j\omega)]|i_{b1}(j\omega)|^2 = \frac{c^2}{c^\lambda}\dot{q}_{b1}.$$
(23)

This shows that if $\lambda < 2$, the higher-capacity cell will always generate more heat since $\dot{q}_{b2}(t)/\dot{q}_{b1}(t) \geq c^{(2-\lambda)} > 1$. However, if $\lambda \geq 2$, the lower-capacity cell may generate more heat due to its high resistance. However, when the current contains significant high-frequency components, the current is distributed according to the cell resistances (i.e., $i_{b2}/i_{b1} \approx c^\lambda$), as mentioned above. Hence, the higher-capacity cell will generate more heat as $\dot{q}_{b2}(t)/\dot{q}_{b1}(t) \approx c^\lambda > 1$, and the higher-capacity cell will have a higher temperature when the cooling conditions for the two cells are the same.

Incorporating Eqs. (3) and (21), the SoC variations of two cells can be derived as:

$$\Delta SoC_1(s) = \frac{cZ_2(s) + c\frac{a\eta}{sQ_{b2}}}{(1 + c^\lambda)Z_2(s) + (1 + c)\frac{a\eta}{sQ_{b2}}}\frac{a\eta}{sQ_{b2}},$$

$$\Delta SoC_2(s) = \frac{c^\lambda Z_2(s) + c\frac{a\eta}{sQ_{b2}}}{(1 + c^\lambda)Z_2(s) + (1 + c)\frac{a\eta}{sQ_{b2}}}\frac{a\eta}{sQ_{b2}}.$$
(24)

Therefore, when $\lambda > 1$, the SoC variation of higher-capacity cell (ΔSoC_2) is larger than that of the lower-capacity cell (ΔSoC_1). Since they have the same initial SoC, the higher-capacity cell is more vulnerable to over-discharge and over-charge. However, when appropriate control algorithm is used, the upper and lower voltages can be imposed as controls and therefore the potential over-charge and over-discharge can be avoided. The complexity of the control algorithm depends on how significant the degradation in OCV is. When $\lambda = 1$, the battery cells have the same SoC (i.e., $SoC_1 = SoC_2$), as the current is always distributed according to the cell capacities (i.e., $Q_{b2}/Q_{b1} = i_{b2}/i_{b1} = c$).

3.2. Cell-to-cell variation of degradation

The temperatures of the two cells are assumed to be the same to simplify the analysis. Based on the degradation model (see Eq. (13)), the degradation rates of different cells and the corresponding ratio can be derived as:

$$\begin{cases} Q_{\text{loss}1} = |i_{b1}|T_s zA^{\frac{1}{z}}e^{-\left(\frac{E_a - B\cdot\frac{|i_{b1}|}{Q_{b1}}}{zRT_b}\right)}\left(1 - \frac{Q_{b1}}{Q_0}\right)^{\frac{z-1}{z}}, \\ Q_{\text{loss}2} = |i_{b2}|T_s zA^{\frac{1}{z}}e^{-\left(\frac{E_a - B\cdot\frac{|i_{b2}|}{Q_{b2}}}{zRT_b}\right)}\left(1 - \frac{Q_{b2}}{Q_0}\right)^{\frac{z-1}{z}}, \end{cases}$$
(25)

$$\frac{Q_{\text{loss1}}}{Q_{\text{loss2}}} = \frac{|i_{\text{b1}}|}{|i_{\text{b2}}|} e^{\left(\frac{E_a - B \cdot \frac{|i_{\text{b2}}|}{Q_{\text{b2}}}}{zRT_{\text{b}}}\right) - \left(\frac{E_a - B \cdot \frac{|i_{\text{b1}}|}{Q_{\text{b1}}}}{zRT_{\text{b}}}\right)} \left(\frac{Q_0 - Q_{\text{b1}}}{Q_0 - cQ_{\text{b1}}}\right)^{\frac{z-1}{z}}. \tag{26}$$

Since generally $E_a \gg B > R > 0$ [11], it can be verified that, when $z \leq 1$, $Q_{\text{loss1}}/Q_{\text{loss2}} < 1$, meaning that the higher-capacity cell (i.e., cell #2) has a higher degradation rate when compared to the lower-capacity cell (i.e., cell #1). Therefore, the cell-to-cell variation of capacity will decrease over time, and it is verified that battery cells with non-concave (i.e., $z \leq 1$) degradation characteristics have a self-balancing mechanism (i.e., the capacities converge over time without control efforts) when they are connected in parallel. We point out that, even when the battery cell has a concave degradation curve (i.e., $z > 1$), the self-balancing mechanism may also be preserved, but it depends on how concave the degradation curve is (i.e., the value of z). Specifically, given the same current, the cell will have less, same, and more degradation via aging when the degradation curve is convex, linear, and concave, respectively. In addition, the lower-capacity cell in a parallel battery string has less current given its larger resistance. As a result, the cell-to-cell variation will converge to 0 for parallel-connected cells with non-concave degradation curves.

The temperature distribution is assumed to be homogeneous in the above analysis. Note that in practical applications, it is challenging to keep all temperatures same. But it is reasonable to assume similar cooling conditions for different cells as the cooling system is generally designed for this purpose. As illustrated in

Currently, battery manufacturers make massive efforts to keep the individual cells consistent and ensure that vehicle manufacturers can assemble battery packs with uniform cells. But the benefit of doing so is not obvious; therefore, the impact of cell-to-cell variation on pack aging is quantified in this study. Based on Eq. (16), the capacity variation Q_{var} can be defined as:

$$Q_{\text{var}} = \frac{Q_{\text{b2}} - Q_{\text{b1}}}{2} \tag{27}$$

And we have

$$Q_{\text{var}} = \frac{Q_{\text{bs}}}{2} - Q_{\text{b1}} = Q_{\text{b2}} - \frac{Q_{\text{bs}}}{2} \tag{28}$$

Given a constant current i_{b}, the total degradation of the battery string during one sampling period can be formulated as

$$\Delta Q_{\text{tot}} = \sum_{i=1}^{2} |i_{\text{b}i}| T_s z A^{\frac{1}{z}} e^{-\left(\frac{E_a - B \cdot \frac{|i_{\text{b}i}|}{Q_{\text{b}i}}}{zRT_{\text{b}i}}\right)} \left(1 - \frac{Q_{\text{b}i}}{Q_0}\right)^{\frac{z-1}{z}} \text{ with } Q_{\text{b1}} \in \left(0, \frac{Q_{\text{bs}}}{2}\right) \tag{29}$$

where ΔQ_{tot} is the total degradation of battery string. The relationship between cell-to-cell variation and total degradation of the battery string can be obtained based on Eqs. (28) and (29). Then the impact of cell-to-cell variation can be quantified by differentiating Eq. (29) as follows

$$\frac{\partial \Delta Q_{\text{tot}}}{\partial Q_{\text{var}}} = -\frac{\partial Q_{\text{loss1}}}{\partial Q_{\text{b1}}} + \frac{\partial Q_{\text{loss2}}}{\partial Q_{\text{b2}}}$$

$$= \frac{\partial |i_{\text{b2}}|}{\partial Q_{\text{b2}}} T_s z A^{\frac{1}{z}} e^{-\left(\frac{E_a - B \cdot \frac{|i_{\text{b2}}|}{Q_{\text{b2}}}}{zRT_{\text{b}}}\right)} \left(1 - \frac{Q_{\text{b2}}}{Q_0}\right)^{\frac{z-1}{z}} - \frac{\partial |i_{\text{b1}}|}{\partial Q_{\text{b1}}} T_s z A^{\frac{1}{z}} e^{-\left(\frac{E_a - B \cdot \frac{|i_{\text{b1}}|}{Q_{\text{b1}}}}{zRT_{\text{b}}}\right)} \left(1 - \frac{Q_{\text{b1}}}{Q_0}\right)^{\frac{z-1}{z}}$$

$$+ |i_{\text{b2}}| T_s z A^{\frac{1}{z}} e^{-\left(\frac{E_a - B \cdot \frac{|i_{\text{b2}}|}{Q_{\text{b2}}}}{zRT_{\text{b}}}\right)} \left(\frac{1-z}{z}\right) \left(\frac{1}{Q_0}\right) \left(1 - \frac{Q_{\text{b2}}}{Q_0}\right)^{-\frac{1}{z}} - |i_{\text{b1}}| T_s z A^{\frac{1}{z}} e^{-\left(\frac{E_a - B \cdot \frac{|i_{\text{b1}}|}{Q_{\text{b1}}}}{zRT_{\text{b}}}\right)} \left(\frac{1-z}{z}\right) \left(\frac{1}{Q_0}\right) \left(1 - \frac{Q_{\text{b1}}}{Q_0}\right)^{-\frac{1}{z}} \tag{30}$$

$$+ \frac{|i_{\text{b2}}|}{Q_{\text{b2}}} T_s z A^{\frac{1}{z}} e^{-\left(\frac{E_a - B \cdot \frac{|i_{\text{b2}}|}{Q_{\text{b2}}}}{zRT_{\text{b}}}\right)} \frac{B}{zRT_{\text{b}}} \left(\frac{\partial |i_{\text{b2}}|}{\partial Q_{\text{b2}}} - \frac{|i_{\text{b2}}|}{Q_{\text{b2}}}\right) \left(1 - \frac{Q_{\text{b2}}}{Q_0}\right)^{\frac{z-1}{z}} - \frac{|i_{\text{b1}}|}{Q_{\text{b1}}} T_s z A^{\frac{1}{z}} e^{-\left(\frac{E_a - B \cdot \frac{|i_{\text{b1}}|}{Q_{\text{b1}}}}{zRT_{\text{b}}}\right)} \frac{B}{zRT_{\text{b}}} \left(\frac{\partial |i_{\text{b1}}|}{\partial Q_{\text{b1}}} - \frac{|i_{\text{b1}}|}{Q_{\text{b1}}}\right) \left(1 - \frac{Q_{\text{b1}}}{Q_0}\right)^{\frac{z-1}{z}}.$$

Section 3.1, a higher-capacity cell will have a higher temperature due to its higher current, assuming the cooling conditions of different cells are the same. The battery resistance will decrease with the increasing temperature [29]. Therefore, current imbalance is enhanced by the higher temperature of the higher-capacity cell, and will induce a faster convergence of cell-to-cell variation. All conclusions derived from above analysis are still valid. Note that the battery degradation model shown in Section 2.2 adopts the normalized C rate rather than the absolute of current, and the increase in temperature (not current) of the higher-capacity cell will be the main reason for speeding up the self-balancing process.

It can be proven that, when $z \leq 1$, the first and second terms of the expression are positive, while the third term depends on the value of λ, indicating the characteristics of the resistance-degradation curve. Specifically, when $\lambda = 1$, the resistance increases linearly with degradation and it can be proven that the third term in Eq. (30) is 0. As a result, we can prove $\partial \Delta Q_{\text{tot}}/\partial Q_{\text{var}} > 0$, meaning that a cell-to-cell variation will increase the total degradation of the battery string and therefore there is a benefit to assemble the cells with the same capacity in one string. Even though $\lambda = 1$ is a special case, the analysis presented in Ref. [28] found that the battery resistance increases "linearly" (i.e., $\lambda \approx 1$) in

Table 1
Simulation parameters.

Parameter	Value
Cell nominal capacity (Ah)	60
Cell ohmic resistance R_s (mΩ)	~1
Cell diffusion resistance R_t (mΩ)	~1
Cell time constant τ (s)	4
OCV-SoC ratio a (mV/%)	~1.5
Pre-exponential factor A	0.0032
Compensation factor B	1516
Activation energy E_a (J)	15162
Time factor z	0.824
Gas constant R (J/(mol · K))	8.314
Cell thermal capacity C_b (J/K)	2300
Heat transfer coefficient h_b (W/K)	5
Ambient temperature (°C)	25
Constant coefficient ε	1.2
Constant coefficient λ	2
Constant coefficient η	0.99
Sampling time (s)	30

the normal operation range before the highly nonlinear region near end-of-life. However, when $\lambda > 1$ the resistance increases convexly with degradation, and so the third term depends on the total current and the battery parameters (could be positive, negative, or 0). In this case $\partial \Delta Q_{tot}/\partial Q_{var} > 0$ may be preserved but is difficult to be rigorously proven.

Based on the above analysis, two remarks can be given.

Remark 1. When the cell has convex or linear degradation characteristics, cell-to-cell variation within parallel-connected cells will naturally decrease (i.e., self-balancing). The convergence accelerates with a more linear cell degradation curve (i.e., z approaches to 1).

Remark 2. The total degradation of the battery string is minimized when the same cells (i.e., no cell-to-cell variation) are adopted.

4. Simulation results

To further verify the insights given in Section 3, a simulation is conducted considering battery strings including more cells (i.e., 5 cells in one string). 60 A h LiFePO$_4$ cells are used in the simulation; detailed information on this cell is given in Refs. [11,29]. It is assumed that all cells have the same cooling condition (i.e., the same heat transfer coefficient), and the ambient temperature (i.e., the initial temperature of the cells) is 25 °C. The relationship between temperature and cell resistance is quantified as

$$\begin{cases} R_{si} = [1 - \eta(T_{bi} - T_{b0})]R_{s0}, \\ R_{ti} = [1 - \eta(T_{bi} - T_{b0})]R_{t0}, \end{cases} \tag{31}$$

where T_{b0} is the temperature at which the baseline resistance is calibrated, and η is a constant coefficient which is positive as the battery resistance decreases with the increasing temperature. The

Table 2
Three battery strings considered in simulation.

	String #1	String #2	String #3
Cell #1 (Ah)	60.44560	59.53430	58.68382
Cell #2 (Ah)	60.14180	58.92680	58.68382
Cell #3 (Ah)	58.92680	58.92680	58.68382
Cell #4 (Ah)	57.10430	58.31930	58.68382
Cell #5 (Ah)	56.80060	57.71180	58.68382
Total capacity (Ah)	293.4191	293.4191	293.4191
Capacity variation (Ah^2)	2.8324	0.4798	0

specifications for the simulation are listed in Table 1. Note that the adopted battery cell has a convex degradation curve since $z < 1$.

An electric model achieved by discretizing Eqs. (6) and (7), the aging model shown in Eq. (3), and the thermal model shown in Eq. (15) are used in the simulation. Given that battery degradation is a long-term process, the sampling time is set to 30s in the simulation without losing accuracy. We point out that in general one does not cycle a LiFePO$_4$ battery at high current, as it will induce significant degradation. However, in this simulation the battery string is discharging and charging repeatedly at a 6C rate with an initial SoC of 60% to expedite the degradation. We point out that this is the accelerated aging test and will not occur in practical EV applications where the maximum battery current is below 2C [39]. As the battery degradation is a long-term issue, there is a trade-off between simulation time and accuracy. When the current is increased to 6C, the simulation time can be significantly reduced, which is the main consideration of this study to use aggressive current profile to speed up the simulation process. When the current profile changes, the degradation processes of different cells will change accordingly, but all conclusions in the following analysis will be preserved. We point out that the adopted current profile will not make battery violate any operation constraint. Three battery strings with the same total capacity and different capacity variations are considered, as listed in Table 2, to investigate the cell-to-cell convergence and its impact on total degradation of battery strings. The capacity variation among different cells is defined as:

$$Q_{sv} = \frac{1}{N-1} \sum_{i=1}^{N} \left[Q_{bi} - \frac{1}{N} \sum_{i=1}^{N} (Q_{bi}) \right]^2, \tag{32}$$

where Q_{sv} denotes the capacity variation (Ah^2) and N is the cell number (i.e., 5). Based on the thermal electric aging model introduced in Section 2, the simulation for string #1 is conducted under the current profile shown in Fig. 3. The current amplitude decreases with battery aging to achieve a constant C rate.

As shown in Fig. 4(a), the higher-capacity cells (i.e., cell #1 and cell #2) degrade faster than the lower-capacity cells (e.g., cell #5). As a result, the cell-to-cell variation almost converges to 0 after 300 h of operation, as shown in Fig. 4(b). Therefore the analysis of the convergence of cell-to-cell variation provided in Section 3.2 is verified. In addition, under the same cooling conditions, the higher-capacity cells have a higher temperature initially due to their larger currents. With the decreasing cell-to-cell variation, the current is distributed more evenly, and therefore the temperatures of different cells converge to the same value ultimately, as shown in Fig. 4(c). The SoC of the higher-capacity cells vary over a wider range when compared to the lower-capacity cells, as shown in Fig. 4(d). The higher-capacity cells are discharged and charged more quickly than the lower-capacity cells, as shown in Eq. (22). Since the SoC trajectories are periodic, only a small fraction of them are presented. In this paper, a powerful cooling system is incorporated in the simulation to control the battery temperature under this aggressive current profile, which is chosen to reduce the simulation time. The strong cooling system indicates a lower temperature of coolant or a higher flow rate of coolant, which can increase the heat transfer between cells and coolant. We point out that in practical applications the strong cooling system may not exist. But all conclusions, obtained by the analytical investigation in Section 3, will preserve regardless of the current profile and the cooling capacity. The numerical analysis in this section is conducted to further verify the above findings.

Note that the current circumfluence may exist among different cells after testing and this was not considered in this paper. As shown in Fig. 4(d), the SoC difference among cells during testing is
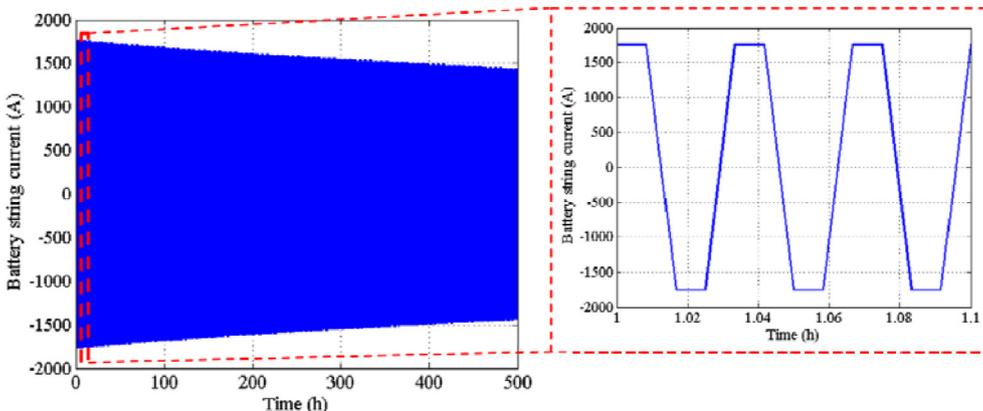
Fig. 3. The current profile for battery cycling.

(a) Cell capacities

(b) Cell-to-cell variation

(c) Cell temperatures

(d) Cell SoC
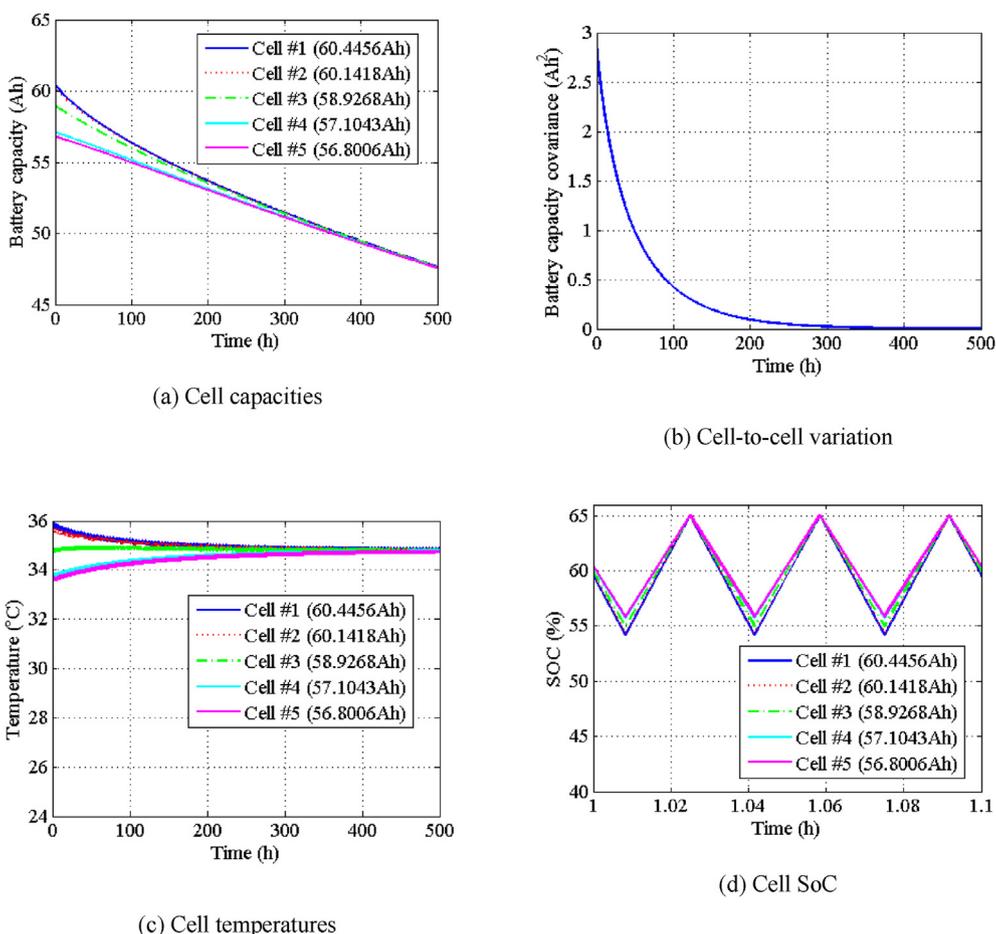
Fig. 4. Simulation results for string #1.

below 3%, which will not cause significant OCV difference (i.e., less than 10 mV) as the OCV-SoC curve is flat. Therefore, the current circumfluence among cells will be no more than 5 A (i.e., 1/12C). In addition, the current circumfluence will not last long after testing. As a result, when compared to the testing current (i.e., 6C), the influence of current circumfluence on variation progression can be neglected.

Another battery string with smaller initial variation (i.e., string #2) is also investigated. As shown in Fig. 5, the capacities of the

different cells converge to the same value and the cell-to-cell variation converges to 0 after around 300 h. Note that convergence will take longer in actual applications since the current will likely be much less than that of the simulations. To evaluate the influence of cell-to-cell variation on the total degradation of the battery string, string #3 including consistent cells is also considered. These 3 battery strings, which have the same total capacity and different initial cell-to-cell variations, are compared under the 500-h cycling simulation. The total degradation values of three
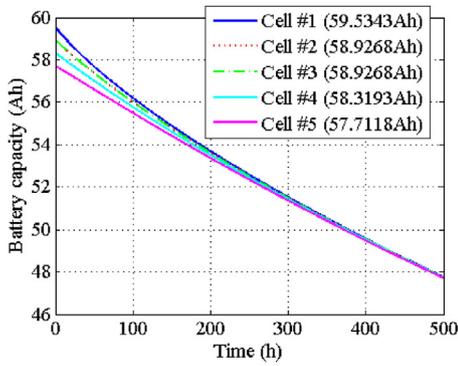
(a) Cell capacities
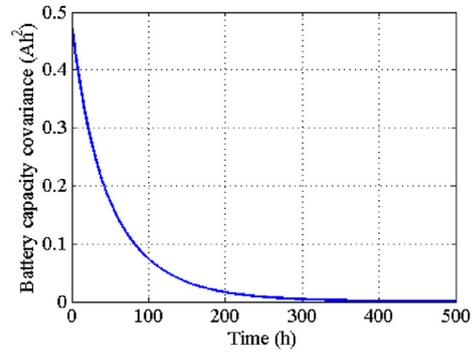
(b) Cell-to-cell variation

Fig. 5. Simulation results for string #2.
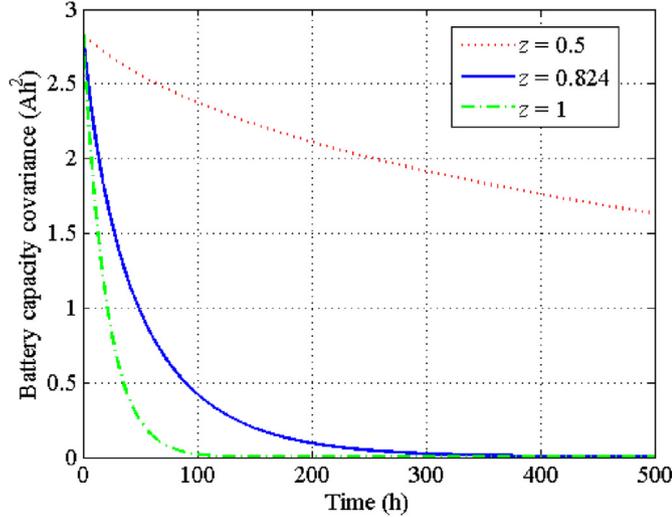
Fig. 6. Effects of z on capacities convergence.
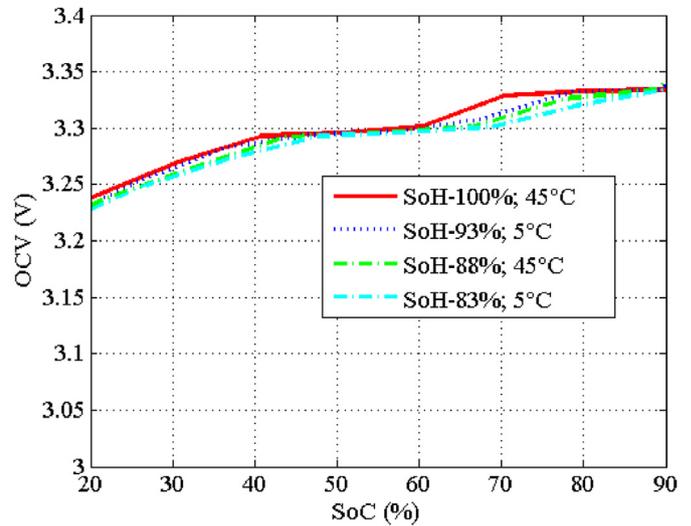
Fig. 7. The OCV-SoC curves of the studied LiFePO$_4$ cell under different SoH and temperatures.

battery strings are 55.3746 A h, 54.8107 A h, and 54.6980 A h, respectively. It shows that the battery string including consistent cells has less total degradation when compared to the battery string with cell-to-cell variation, though the benefit is not significant.

As mentioned in the prequel, the cell degradation characteristics significantly influence the progression of cell-to-cell variation. Therefore, the variation progression of string #1 is evaluated for different z values. First, z is increased from 0.824 to 0.99 so the cell degradation curve is more linear. Based on Eq. (26), the cell-to-cell variation will diminish faster with increasing z. This is also verified in the simulation, as shown in Fig. 6. The convergence time of the cell-to-cell variation decreases from ~300 h to ~100 h. On the other hand, convergence takes longer when z is decreased from 0.824 to 0.5. Based on above analysis and simulation results, we point out that for the battery aging management, consistent cells (i.e., small initial cell-to-cell variation) should be selected for series-connected cells, which should be carefully monitored and controlled in real-time applications. The battery management system should ensure similar degradation rates for all cells. In contrast, the cells connected in parallel can tolerate some initial variations due to the self-
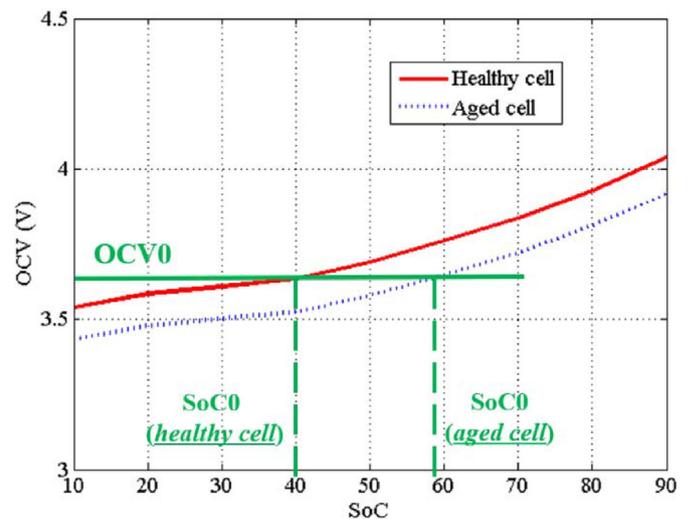
Fig. 8. The degradation of OCV.

balancing mechanism and they cannot be monitored and controlled as there is no controllability.

5. Discussion

5.1. The influence of OCV degradation

In the above analysis, the OCV-SoC curves are assumed to be fixed regardless of temperatures and cell degradation levels. For the studied LiFePO$_4$ cell, there is no significant change in the OCV-SoC curve when the cell ages under different temperatures, as shown in Fig. 7. Even though the OCV at 70% SoC reduces when the cell SoH drops from 100% to 93%, no significant reduction is found afterwards.

Fixed OCV-SoC curves are extensively found for LiFePO$_4$ and NCM cells [40–44]. However, a fixed OCV-SoC curve is not guaranteed for all batteries. For example, the decreasing OCV curves are found for LiFePO$_4$ cell in Ref. [45] and NCM cell in Ref. [46]. A decreasing OCV-SoC curve (i.e., OCV decreases with degradation) is depicted in Fig. 8. We point out that, as long as the OCV-SoC curves can be linearized, which is generally true for LiFePO$_4$ cells, and have the same slopes for the fresh and lower-capacity cells, the provided analysis is valid. For cells with significant nonlinearity and degradation in the OCV-SoC curve, it is difficult to directly generalize the conclusions drawn in this paper.

5.2. Uneven cooling conditions

The cooling condition for different cells is assumed to be same in this paper; however, this is almost impossible to achieve in practical applications. As long as the cooling conditions for different cells are not significantly different, the conclusions drawn in this paper are still valid. And it is desirable to ensure similar cooling conditions for different cells to suppress uneven temperature distributions, which can significantly increase the cell-to-cell variation [5,19].

If some cells are located at a "hotspot" and have much higher temperatures than the other cells, the hot cells will degrade much faster and reach their end of life much earlier. The reasons are 1) the high temperature will induce low resistance and therefore high current, which will significantly increase the degradation; 2) the high temperature also directly increases the degradation [29]. The cooling system design for battery modules is therefore of critical importance; however, this is a separate topic, which will not be covered in this paper.

6. Conclusion

In this paper, the cell-to-cell variation of capacity among parallel-connected battery cells is studied. To investigate the progression of capacity variation, an electric aging model is proposed and analysis is provided. It shows that the progression of cell-to-cell variation highly depends on the cell degradation characteristics. Specifically, when a similar cooling condition can be guaranteed within the battery string, the variation will decrease for cells with convex or linear degradation curves (i.e., the most common ones), meaning that parallel-connected cells have a self-balancing mechanism. In addition, when compared to the battery strings with the same total capacity (i.e., no variation), an initial variation slightly increases the total degradation of the battery string. The higher-capacity cell has a wider SoC trajectory and higher temperature due to higher losses. Simulation results further verify the self-balancing mechanism.

In future work, the lab-level experiment will be conducted to further validate how the cell-to-cell variation progresses within parallel-connected cells. In addition, cell-to-cell variations due to different cooling conditions will be considered, and typical cooling structures will be studied to further investigate the progression of cell-to-cell variation.

CRediT authorship contribution statement

Ziyou Song: Simulation, Analysis, Writing. **Xiao-Guang Yang:** Analysis, Editing, Data Acquisition. **Niankai Yang:** Analysis, Editing. **Fanny Pinto Delgado:** Analysis, Editing. **Heath Hofmann:** Supervision, Analysis, Reviewing and Editing. **Jing Sun:** Supervision, Analysis, Reviewing and Editing.

Declaration of competing interest

None.

Acknowledgement

References

[1] Song Z, Li J, Hou J, Hofmann H, Ouyang M, Du J. The battery-supercapacitor hybrid energy storage system in electric vehicle applications: a case study. Energy 2018;154:433–41.

[2] Song Z, Feng S, Zhang L, Hu Z, Hu X, Yao R. Economy analysis of second-life battery in wind power systems considering battery degradation in dynamic processes: real case scenarios. Appl Energy 2019;251:113411.

[3] Bruen T, Marco J. Modelling and experimental evaluation of parallel connected lithium ion cells for an electric vehicle battery system. J Power Sources 2016;310:91–101.

[4] Pastor-Fernández C, Bruen T, Widanage WD, Gama-Valdez MA, Marco J. A study of cell-to-cell interactions and degradation in parallel strings: implications for the battery management system. J Power Sources 2016;329: 574–85.

[5] Shi W, Hu X, Jin C, Jiang J, Zhang Y, Yip T. Effects of imbalanced currents on large-format LiFePO4/graphite batteries systems connected in parallel. J Power Sources 2016;313:198–204.

[6] Kong X, Zheng Y, Ouyang M, Lu L, Li J, Zhang Z. Fault diagnosis and quantitative analysis of micro-short circuits for lithium-ion batteries in battery packs. J Power Sources 2018;395:358–68.

[7] An F, Huang J, Wang C, Li Z, Zhang J, Wang S, Li P. Cell sorting for parallel lithium-ion battery systems: evaluation based on an electric circuit model. Journal of Energy Storage 2016;6:195–203.

[8] Ahmed S, Nelson PA, Gallagher KG, Dees DW. Energy impact of cathode drying and solvent recovery during lithium-ion battery manufacturing. J Power Sources 2016;322:169–78.

[9] Pesaran AA. Battery thermal models for hybrid vehicle simulations. J Power Sources 2002;110(2):377–82.

[10] Panchal S, Mcgrory J, Kong J, Fraser R, Fowler M, Dincer I, Agelin-Chaab M. Cycling degradation testing and analysis of a LiFePO4 battery at actual conditions. Int J Energy Res 2017;41(15):2565–75.

[11] Song Z, Hofmann H, Li J, Han X, Zhang X, Ouyang M. A comparison study of different semi-active hybrid energy storage system topologies for electric vehicles. J Power Sources 2015;274:400–11.

[12] Lai X, Qiao D, Zheng Y, Ouyang M, Han X, Zhou L. A rapid screening and regrouping approach based on neural networks for large-scale retired lithium-ion cells in second-use applications. J Clean Prod 2019;213:776–91.

[13] Saez-de-Ibarra A, Martinez-Laserna E, Stroe DI, Swierczynski M, Rodriguez P. Sizing study of second life Li-ion batteries for enhancing renewable energy grid integration. IEEE Trans Ind Appl 2016;52(6):4999–5008.

[14] Paul S, Diegelmann C, Kabza H, Tillmetz W. Analysis of ageing inhomogeneities in lithium-ion battery systems. J Power Sources 2013;239: 642–50.

[15] Chiu KC, Lin CH, Yeh SF, Lin YH, Huang CS, Chen KC. Cycle life analysis of series connected lithium-ion batteries with temperature difference. J Power Sources 2014;263:75–84.

[16] Offer GJ, Yufit V, Howey DA, Wu B, Brandon NP. Module design and fault diagnosis in electric vehicle batteries. J Power Sources 2012;206:383–92.

[17] Yang N, Zhang X, Shang B, Li G. Unbalanced discharging and aging due to temperature differences among the cells in a lithium-ion battery pack with parallel combination. J Power Sources 2016;306:733–41.

[18] Gong X, Xiong R, Mi CC. Study of the characteristics of battery packs in electric vehicles with parallel-connected lithium-ion battery cells. IEEE Trans Ind Appl 2014;51(2):1872–9.

[19] Liu X, Ai W, Marlow MN, Patel Y, Wu B. The effect of cell-to-cell variations and thermal gradients on the performance and degradation of lithium-ion battery packs. Appl Energy 2019;248:489−99.

[20] Perez HE, Siegel JB, Lin X, Stefanopoulou AG, Ding Y, Castanier MP. Parameterization and validation of an integrated electro-thermal cylindrical lfp battery model. In: ASME 2012 5th annual dynamic systems and control conference joint with the JSME 2012 11th motion and vibration conference. American Society of Mechanical Engineers Digital Collection; 2012. p. 41−50.

[21] Song Z, Wu X, Li X, Sun J, Hofmann HF, Hou J. Current profile optimization for combined state of charge and state of health estimation of lithium ion battery based on cramer−rao bound analysis. IEEE Trans Power Electron 2018;34(7):7067−78.

[22] Song Z, Wang H, Hou J, Hofmann H, Sun J. Combined state and parameter estimation of lithium-ion battery with active current injection. IEEE Trans Power Electron 2020;35(4):4439−47. https://doi.org/10.1109/TPEL.2019.2945513. In this issue.

[23] Wei J, Dong G, Chen Z. Remaining useful life prediction and state of health diagnosis for lithium-ion batteries using particle filter and support vector regression. IEEE Trans Ind Electron 2017;65(7):5634−43.

[24] Lin X, Perez HE, Mohan S, Siegel JB, Stefanopoulou AG, Ding Y, Castanier MP. A lumped-parameter electro-thermal model for cylindrical batteries. J Power Sources 2014;257:1−11.

[25] Song Z, Hou J, Hofmann HF, Lin X, Sun J. Parameter identification and maximum power estimation of battery/supercapacitor hybrid energy storage system based on cramer−rao bound analysis. IEEE Trans Power Electron 2018;34(5):4831−43.

[26] Hou J, Song Z. A hierarchical energy management strategy for hybrid energy storage via vehicle-to-cloud connectivity. Appl Energy 2020;257:113900.

[27] Yang XG, Leng Y, Zhang G, Ge S, Wang CY. Modeling of lithium plating induced aging of lithium-ion batteries: transition from linear to nonlinear aging. J Power Sources 2017;360:28−40.

[28] Schuster SF, Bach T, Fleder E, Müller J, Brand M, Sextl G, Jossen A. Nonlinear aging characteristics of lithium-ion cells under different operational conditions. Journal of Energy Storage 2015;1:44−53.

[29] Song Z, Li J, Han X, Xu L, Lu L, Ouyang M, Hofmann H. Multi-objective optimization of a semi-active battery/supercapacitor energy storage system for electric vehicles. Appl Energy 2014;135:212−24.

[30] Han X, Ouyang M, Lu L, Li J. A comparative study of commercial lithium ion battery cycle life in electric vehicle: capacity loss estimation. J Power Sources 2014;268:658−69.

[31] Wang J, Liu P, Hicks-Garner J, Sherman E, Soukiazian S, Verbrugge M, Finamore P. Cycle-life model for graphite-LiFePO4 cells. J Power Sources 2011;196(8):3942−8.

[32] Han X, Lu L, Zheng Y, Feng X, Li Z, Li J, Ouyang M. A review on the key issues of the lithium ion battery degradation among the whole life cycle. ETransportation 2019;1:100005.

[33] Forgez C, Do DV, Friedrich G, Morcrette M, Delacourt C. Thermal modeling of a cylindrical LiFePO4/graphite lithium-ion battery. J Power Sources 2010;195(9):2961−8.

[34] Lin X, Fu H, Perez HE, Siege JB, Stefanopoulou AG, Ding Y, Castanier MP. Parameterization and observability analysis of scalable battery clusters for onboard thermal management. Oil & Gas Science and Technology−Revue d'IFP Energies nouvelles 2013;68(1):165−78.

[35] Wang T, Wu X, Xu S, Hofmann H, Du J, Li J, Song Z. Performance of plug-in hybrid electric vehicle under low temperature condition and economy analysis of battery pre-heating. J Power Sources 2018;401:245−54.

[36] Song Z, Hofmann H, Li J, Hou J, Zhang X, Ouyang M. The optimization of a hybrid energy storage system at subzero temperatures: energy management strategy design and battery heating requirement analysis. Appl Energy 2015;159:576−88.

[37] Ouyang M, Chu Z, Lu L, Li J, Han X, Feng X, Liu G. Low temperature aging mechanism identification and lithium deposition in a large format lithium iron phosphate battery for different charge profiles. J Power Sources 2015;286:309−20.

[38] Zhang Y, Wang CY, Tang X. Cycling degradation of an automotive LiFePO4 lithium-ion battery. J Power Sources 2011;196(3):1513−20.

[39] Darcovich K, MacNeil DD, Recoskie S, Kenney B. Coupled electrochemical and thermal battery models for thermal management of prismatic automotive cells. Appl Therm Eng 2018;133:566−75.

[40] Zhang C, Jiang J, Zhang L, Liu S, Wang L, Loh P. A generalized SOC-OCV model for lithium-ion batteries and the SOC estimation for LNMCO battery. Energies 2016;9(11):900.

[41] Yang R, Xiong R, He H, Mu H, Wang C. A novel method on estimating the degradation and state of charge of lithium-ion batteries used for electrical vehicles. Appl Energy 2017;207:336−45.

[42] Shi W, Hu X, Wang J, Jiang J, Zhang Y, Yip T. Analysis of thermal aging paths for large-format LiFePO4/graphite battery. Electrochim Acta 2016;196:13−23.

[43] Weng C, Cui Y, Sun J, Peng H. On-board state of health monitoring of lithium-ion batteries using incremental capacity analysis with support vector regression. J Power Sources 2013;235:36−44.

[44] Yildiz M, Karakoc H, Dincer I. Modeling and validation of temperature changes in a pouch lithium-ion battery at various discharge rates. Int Commun Heat Mass Tran 2016;75:311−4.

[45] Xing Y, He W, Pecht M, Tsui KL. State of charge estimation of lithium-ion batteries using the open-circuit voltage at various ambient temperatures. Appl Energy 2014;113:106−15.

[46] Stroe AI, Knap V, Stroe DI. Comparison of lithium-ion battery performance at beginning-of-life and end-of-life. Microelectron Reliab 2018;88:1251−5.